Payri, R.; Salvador, FJ.; Abboud, R.; Viera, A. (2020). Study of evaporative diesel spray interaction in multiple injections using optical diagnostics. Applied Thermal Engineering. 176:1-12. https://doi.org/10.1016/j.applthermaleng.2020.115402

Study of evaporative Diesel spray interaction in multiple injections using optical diagnostics

Raul Payri[a,*], F. Javier Salvador[a], Rami Abboud[a], Alberto Viera[b]

[a] *CMT - Motores Térmicos, Universitat Politècnica de València, Edificio 6D, 46022, Valencia, Spain.*
[b] *AVL Ibérica SA, Edificio El Rengle Núcleo D, 08302, Mataró, Barcelona*

Abstract

Internal combustion engines have witnessed an ever increasing stringency in emission limits and fuel economy regulations that has continuously provoked researchers to develop complex strategies that enables engines to cope with these standards. Optical techniques have been a viable method in the study of thermal processes occurring inside internal combustion engines and provides researchers with a solid understanding of the heat and mass transfer taking place. In particular, the current study utilizes two optical techniques, diffused back illumination and schlieren imaging, to visualize the spray behavior in multiple injection strategies of evaporative diesel sprays. A novel method has been developed in order to couple the two optical techniques to visualize both liquid and vapor phases of either pilot-main and main-post injections. The influence of the auxiliary injections on the main, and vice versa, in terms of spray segmentation and spray development has been studied for two different pilot/post quantities and four hydraulic dwell times under two different chamber conditions. The spray development displayed no effect of pilot quantity and dwell time on the liquid length of the second injection. On the other hand, a more pronoun effect on the vapor phase penetration and spreading angle was evidenced by the pilot injection where the main injection has penetrated farther with a higher spreading angle as compared to the case with a single injection event. The un-

*Corresponding author. E-mail address: rpayri@mot.upv.es

derstanding of multiple injection is thus fundamental for the improvement of thermal processes in Internal Combustion Engines.

Keywords: Multiple injections, diesel, evaporation, diffused back-illumination, schlieren, optical diagnostics

1. Introduction

As the standards on diesel pollutants control are increasingly restrictive, multiple injection strategies are one of the numerous techniques/technologies used to reduce its emissions [1, 2]. A typical injection event consist of a single and continuous supply of fuel to the combustion chamber. With multiple injections, as the name suggests, the fuel is divided into many dosed quantities, that can be either equal in mass (split strategy) or different (early-pilot-post-late strategies). The main difference between the last two strategies is that the split injections generally divide the target mass uniformly across different pulses. Contrarily, in multiple injections with a main, each auxiliary pulse can be of a different quantity, trying to match the same injected target mass as a single injection event, to prevent increasing fuel consumption. In general, the distance between pulses is referred to as the dwell time (DT). It is important to remark that the real dwell time is the separation between mass flow rate pulses and not the command signal, to consider the hydraulic delay of the start and end of injection.

The number of pulses is limited to the capabilities of the injection system and the duration of the combustion. However, as the diesel technology evolves, newer injection systems allow to precisely inject up to 8 different times per cycle [3]. More pulses provide more flexibility and control over the heat release and air-fuel mixing process, which if tuned properly, can lead to a better engine performance [4].

Over the years, researchers have studied diesel sprays to understand the mechanisms involved in its development. More precisely, Chen et al. [5] inves-

tigated the impact of wall temperature on the diesel spray characteristics identifying that liquid phase is almost unaltered as wall temperature is increased, while the region rich in vapor fuel moves closer to the wall. However, effects of wall temperature on soot and ignition delay were more clearly shown in cases with a lower chamber pressure when the liquid phase impinges on the wall. Similarly, Lui et al. [6] showed that with increased injection pressures, the effect of wall temperature on fuel evaporation decreased. Furthermore, multiple injection strategies add an extra degree of complexity, as the interaction between pulses needs to be accounted for. Pressure waves induced by an injection could alter the injected quantity in the following stage if no tuning measures to the energizing time were taken [7] . In such sense, computational fluid dynamics (CFD) or even simple 1-D spray models offer unmatched advantages [8], as they can provide a detailed spatial description of variables, which are experimentally unmeasurable, with a high temporal resolution. Nevertheless, models are often limited to high-fidelity experimental data for validation, and these regularly provide results of a single spray contour, even if two injections coexist in the combustion chamber [9, 10].

To this end, experimental measurements of the liquid and vapor phase penetrations were carried out for two simple multiple injection strategies: a pilot-main, and a main-post. The experimental campaign consisted on visualizing the spray development with a diffused back-illumination (DBI) setup coupled with a single-pass schlieren arrangement in an optically accessible high pressure and temperature vessel. Different pilot/post quantities and dwell times were tested, with all conditions always compared to a reference single injection case. A new image processing methodology was used to decouple two sprays that coexist in the same frame, which can provide contour information of two or more injections that are within the field of view of the image.

Therefore, the aims of this paper is to utilize a novel image processing technique able to depict two sprays that coexist in a single frame to investigate the influence of pilot/post injection on the main injection's macroscopic variables as well as the thermal aspects along the spray development. The impact of dwell

time and pilot/post injection masses are to be carefully assessed on both, the optical procedure and the main injection's variables.

Nomenclature

1-D One-Dimensional	EOI End of injection
CFD Computational fluid dynamics	LED Light emitting diode
CPF Constant pressure and flow	OEM Original equipment manufacturer
DBI Diffused back-illumination	PCR Piezo common-rail
DT Dwell time	ROI Rate of injection
ECN Engine combustion network	SOI Start of injection
EGR Exhaust gas recirculation	

2. Materials and methods

This section describes the experimental equipment, test matrix, optical setup, and image processing methodology for the multiple injection strategies measurements.

2.1. Fuel delivery system

The injection system is composed of commercially available components adapted for laboratory use, which are mainly based on a high pressure pump, a common rail equipped with a pressure regulator and the injector.

The injector unit used is the most recent iteration of a commercially available piezo common-rail (PCR) type 5 from Continental [3]. This injector is particularly chosen as a continuation of a previous study carried out on mass flow and momentum flux measurements for multiple injections [7].Its piezo stack actuator makes it possible to improve its efficiency in multiple injection strategies. Moreover, the piezo stack is powerful enough to handle operating injection pressures up to 250 MPa. The injector was fitted out with a custom geometry

six hole nozzle distributed as shown in Figure 1, with a spray optically isolated from the others, labeled spray of interest (SpI) and numbered as plume 1. The main geometrical features of the nozzle provided by the manufacturer are summarized in Table 1.

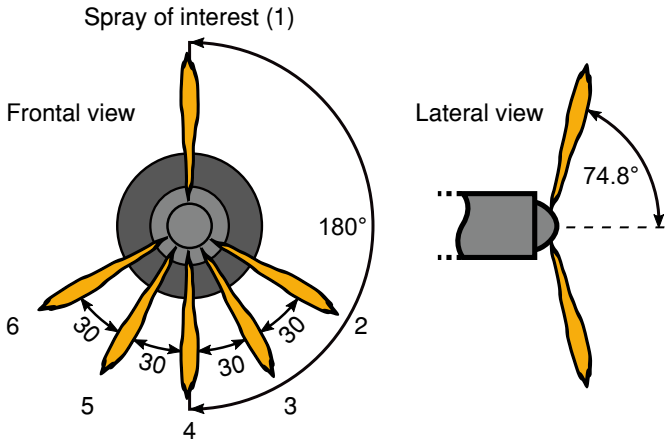

Figure 1: Nozzle configuration of the Continental PCR5 injector used.

Table 1: Real nozzle geometry.

Parameter	**Value**	**Units**
Number of holes	6	-
Avg. outlet diameter ($\overline{D}_o$)	90.1	μm
Outlet diameter (D_o)	91.7	μm
Avg. $k - factor$	5.3	-
Nominal flow rate	313*	$mL\,min^{-1}$
Avg. heigth angle	74.8	$degrees$
Degree of hydro-erosion	7.7	%

* At 10 MPa of injection pressure.

2.2. Description of the facility

Regarding the spray visualization measurements, a high-pressure and high-temperature facility was used similar to those described in other experimental

works [11, 12]. According to the convention introduced by Baert et al. [13], the installation is equipped with an optically accessible constant pressure and flow (CPF) test chamber (spray box), where typical engine operating conditions are reached due to a continuous flow of high-pressure and high-temperature gas. Consequently, the test chamber can achieve a nearly quiescent and steady thermodynamic environment, and thus, measurements can be performed with a much higher injection frequency, reducing testing time [14].

A schematic diagram of the facility is presented in Figure 2. Two possible configurations could be depicted: open-loop and closed-loop. In the first, the circuit valves are set so that air is filtered, compressed and stored in the high-pressure reservoirs. After lowering its humidity with a high-pressure industrial dryer, it enters the test chamber through a 40 kW electric heating system. Hot gases exit the vessel and, after being cooled down, are ejected into the atmosphere. A second valve, manually operated to control the gas flow, is located downstream of the test chamber. With the correct combination of the circuit valves, the closed-loop configuration could be used to simulate exhaust gas recirculation (EGR), by the addition of nitrogen and continuous monitoring of the oxygen concentration. In addition, this configuration also allows using pure nitrogen for spray measurements in a non-reactive atmosphere.

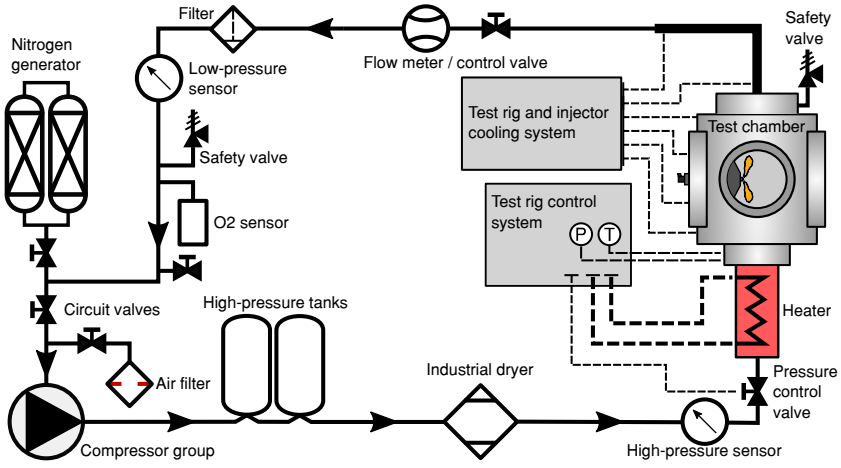

Figure 2: Schematic diagram of the high-temperature and high-pressure facility.

The test rig control system is in charge of regulating both chamber temperature and pressure, where both signals are measured in the combustion chamber. Compared to similar CPF test chambers [14], this spray box features a combustion chamber that reaches temperatures up to 1100 K and 15 MPa, respectively. The test section has a cubic shape of approximately 15 liters in volume. The chamber is optically accessible through three windows, two of 128 mm in diameter located in a line-of-sight arrangement, and one of 181 mm in diameter perpendicular to the axis of the injector. The latter access is thought for industrial injectors, with measurable spray penetrations of up to 110 mm. Details of this facility are thoroughly explained in [15, 16].

2.3. Test matrix

The injection scheduling was setup to optically analyze the interaction between two sprays, either a pilot before the main injection or a main injection on a post. A test group consisted of a single injection event with fixed boundary conditions, and then two different pilot/post quantities and four hydraulic dwell times. Each group was assessed for two rail pressures, two chamber densities and temperatures. Commercially available diesel was used as fuel. The test plan is presented in Table 2.

The proposed test matrix consisted of 72 test points, with ten repetitions per condition. Rail pressures, chamber densities, and temperatures were selected considering engine-relevant conditions from the ECN guidelines [17]. The discharge pressure was set to achieve the target density for a given chamber temperature. The non-reactive atmosphere was achieved using pure nitrogen as the running gas in the facility, which reduced oxygen concentration to nearly zero. A modification to the injector holder was done to approximately achieve same cooling surface and control the operating temperature of the injector, as the heat produced by the piezo stack can affect its dynamic response, and thus, modify the injected quantity of the pilot/post pulses [18].

The total injected mass was selected accounting for a nozzle with a total nominal flow area of 0.06283 mm^2 installed in 1.6 L engine that injects 50

Table 2: Test plan for the non-reactive evaporative spray visualization campaign.

Parameter	**Value**	**Units**
Rail pressure (P_r)	100 - 200	MPa
Chamber density (ρ)	15.2 - 22.8	$\mathrm{kg\,m^{-3}}$
Chamber temperature (T)	800 - 900	K
Oxygen concentration	≈ 0	%
Injector operating temperature	363	K
Pilot/post dwell times	200 - 350 - 500 - 650	µs
Pilot/post injected quantity	1 - 3	mg
Total mass per injection	30	mg
Injection frequency	1	Hz
Repetitions	10	-

mg. The pilot/post mass distribution was chosen considering 5% and 10% of the total injected mass, although in the first case it was reduced to 1 *mg* to amplify the difference between injected quantities. Dwell times were selected considering a minimum hydraulic separation between injection pulses of 200 μs, with increments of 150 up to 650 μs.

The injector was driven with a two-stage voltage signal per injection pulse. The signal is comprised of a boost stage to aid needle lift, and then a hold-off stage that controls injection duration. Voltage levels and ramp-off (volts per second) were provided by the original equipment manufacturer (OEM) and they depend on the injection pressure.

2.4. Optical configuration

Liquid phase penetration is often used in the literature to characterize the mixing process in diesel sprays [19, 20] and it can be observed through several optical configurations that use visible-wavelength light as the source of illumination [16, 20]. Light scattering techniques are an example of such methods and they capture the rays elastically scattered by the droplets through a high-

speed camera [16]. Another method, commonly used with nozzles that allow line-of-sight visualization is diffused-back illumination (DBI), in which light is extinct due to the optical depth (τ) of the spray. The recent introduction of fast light-emitting diodes (LED) allowed to improve the quality of images captured by DBI. As the duration of the light pulse can be set to very low values (nanoseconds), the amount of light available for each frame is governed by the pulse length of the LED, and not the exposure of the camera. Consequently, a DBI configuration was selected for the liquid phase visualization as the images gathered are significantly sharper compared to other continuous light source options [20]. A comparison of this technique among eight others could be found in Pickett et al. [21].

On the other hand, researchers have used schlieren imaging for many years to analyze diesel spray evolution in both non-reactive and reactive conditions. With this technique it is possible to measure complex combustion variables, such as ignition delay [22, 23] and lift-off length [24], from simple macroscopic parameters, mainly vapor phase penetration and spreading angle [25]. It is not only fundamental knowledge to understand how boundary conditions affect these variables, but the experimental data is necessary to validate computational tools, such as 1-D or 3D CFD models. The principle of the schlieren application in diesel sprays is straightforward: the density gradients between the injected fuel and the gas, along the optical path, bend the light rays passing through the test section. Subsequently, the boundary between these elements can be depicted, allowing to segment the diesel spray from the background [26].

The optical configuration used is shown in Figure 3. As the nozzle had an optically isolated plume, both DBI and single-pass schlieren setups were coupled to measure liquid as well as vapor phase development in the same injection event. Two 50:50 beam splitters were needed two enable both setups to access the test section through the same optical accesses, while keeping all the optical axes aligned. The light pulse from the LED (set to 200 ns) was synchronized with the exposure cycles of the Photron SA-X2 camera. In this way, DBI illumination does not interfere with the schlieren configuration, as

the exposure event of the SA5 camera occurs in a different time lapse in the frame of the video. Contrarily, the continuous light from the schlieren setup can be reflected by the optical elements and be visualized in the DBI camera. Moreover, as this light source is collimated, beam steering effects are very likely to appear in the DBI caused by these reflections. Thus a narrow band-pass filter of 460 ± 5 nm, equally centered as the blue LED, was used to minimize the interference of the schlieren light in the liquid visualization. Both cameras were set to start recording with the start of energizing of the injector.

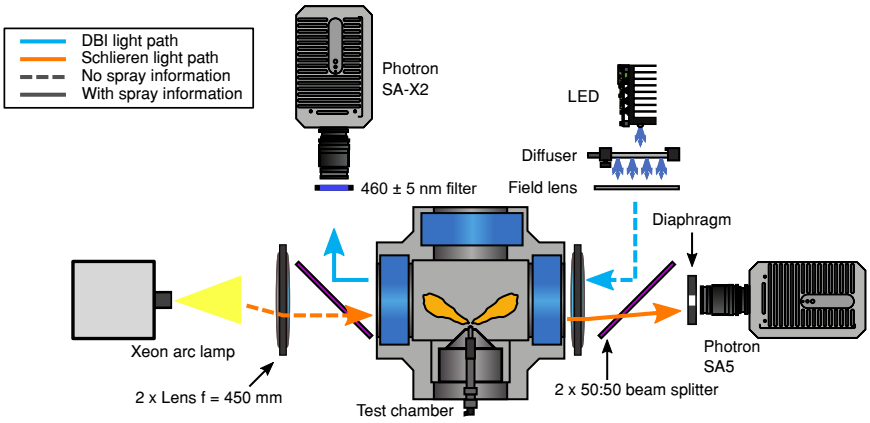

Figure 3: Schematic representation of the optical configuration used for the spray diagnostics.

2.5. Image processing methodology for single injections

The methodology for image processing depends significantly on the parameters to be extracted from the images measured. For most optical diagnostic methods, the primary objective is the segmentation of the spray and the background. Once segmented, a post-analysis of the contour can provide the variables of interest, for instance, spray penetration, spreading angle, or ignition delay, among others. The image processing methodology used for time-resolved movies is composed of four main steps per frame (time-step): image masking, background subtraction, contour detection, and contour analysis. All the routines were programmed in MATLAB.

2.5.1. Image masking

Once read by the software, an image consists of a matrix where the number of rows and columns is the height and width in pixels, respectively. The value of each cell represents the normalized gray scale intensity from black to white (0 - 1).

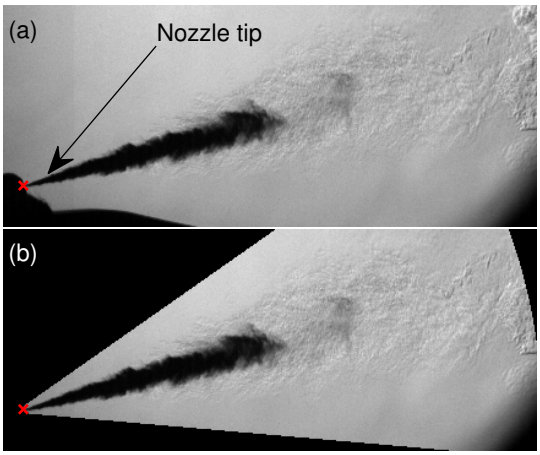

Figure 4: Example of the masking process. The raw and masked images are presented left and right, respectively. The frame shown is at 635 µs after SOI, for a rail pressure of 100 MPa, a chamber density of 15.2 kg m^{-3} and temperature of 800 K.

Image masking consists of providing the processing routine with a region of interest where the spray is located. Therefore, undesired elements present in the frame are discarded for the segmentation, such as window limits, nozzle tip, injector holder, among others, as depicted in Figure 4. The mask is a zero-filled-matrix with dimensions of equal size to the image. The region of interest is represented by cells with a value of 1.

2.5.2. Background subtraction

With the frame masked, the next step in the image processing is the segmentation between the spray and the background. This is a very straightforward task for DBI images, on the contrary, the process is more complicated for schlieren imaging since any density gradient that is detected by the rays

beaming across the test section could be visualized by the setup. As a result, the images gathered could have very distinctive background patterns that might present pixel structures of the same intensity as the spray, and those might move throughout the injection event.

The procedure used to depict the spray contour is a composition of two extensively used approaches, and it is thoroughly described in the work of Payri et al. [27]. The core of the segmentation algorithm is based on a dynamic-background-composition subtraction [25, 27]. To improve its capabilities, it was combined with an image-temporal-derivative approach [27, 28]. Each method produces gray-scale images, which are then combined with an adjustable weighted average.

For multi-injection, a new methodology was developed to decouple the schlieren contour of the auxiliary injections (pilot or post) from the main. In these cases, the difficulty is that the second pulse occurs in conditions where density gradients are already induced by the previous injection. To overcome this problem, the same dynamic background subtraction strategy was applied to the second injection pulse, where the non-spray pixels of the composed background include the image with the first injections, and the remnant pixels, which were identified as the spray in the previous frame, were filled with the original background before injection. The methodology is explained in more detail in [15].

2.5.3. Contour detection

With the spray mostly segmented from the background, its boundary was obtained by binarizing the image with a certain intensity level. For DBI movies, a fixed value of optical thickness was used [25]. In contrast, for schlieren images, the threshold was calculated as a fixed factor multiplied by the dynamic range of the frame being analyzed [19, 25, 27]. Contour detection can be very dependent on the binarization level, and consequently, on the quality of the frames gathered. One example is DBI movies with beam-steering near the tip of the liquid phase jet [29]. Therefore, it is important for images to present sharp edges and a rapid intensity decay near the head of the spray.

Nevertheless, the background subtraction is not perfect, and some structures could have enough intensity to be assigned as the spray in the binarization threshold. Thus, these are removed through a filtering process that consists of erosion-dilation strategies, removal of small pixel areas, and pixel-connectivity criteria [25, 27]. Figure 5 presents an example of the procedure for the frame depicted in Figure 5.*a*, and is as follows:

- Figure 5.*b*: frame after the binarization. For illustration purposes, the threshold was lowered to increase background noise.
- Figure 5.*c*: a two-step erosion that reduced background noise, as well as spray contour dimensions.
- Figure 5.*d*: all the isolated pixel areas that are below a minimum pixel count are removed. The value is arbitrary and was reduced for the early stages of spray development, where its area is small too.
- Figure 5.*e*: a two-step dilation, to counteract the effect of the erosion on the true dimensions of the spray contour.
- Figure 5.*f*: pixel-connectivity criteria, to remove any remaining background in the binarized image. For early stages, the non-spray regions are filtered by selecting the contour nearest to the nozzle exit. At later stages in the injection event, the biggest area in terms of pixel count is selected as spray. The contour is calculated as the coordinates of the pixels in the boundary between the black and white regions.

2.5.4. Contour analysis

Once the boundary was obtained, macroscopic spray variables were calculated for each time step, as shown in Figure 6. Both liquid and vapor phase penetration were defined as the furthest pixel in the radial direction from the nozzle outlet [19, 27, 28], from the DBI and schlieren images respectively. The spreading angle was measured as the angle between two linear fits, calculated at

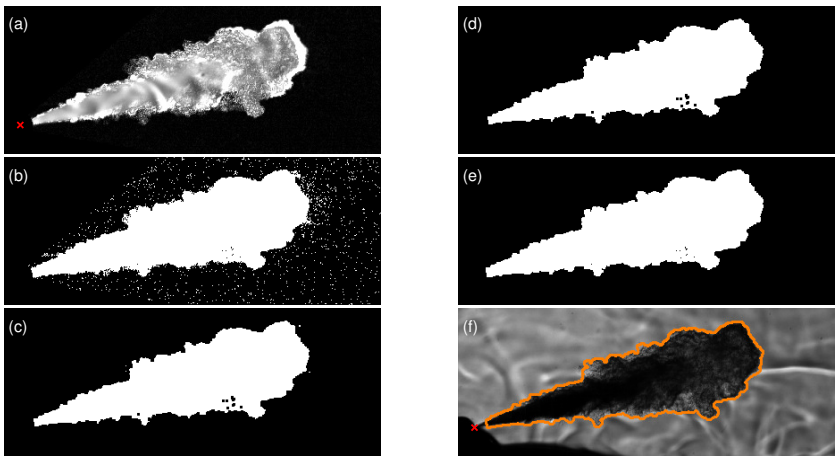

Figure 5: Example of the contour detection algorithm. The frame shown is at 560 µs after SOI, for a rail pressure of 100 MPa, a chamber density of 22.8 kg m^{-3} and temperature of 800 K.

the top and bottom profiles of the spray divided through its axis [20, 25, 27]. The linear fits were computed with all the contour data contained between $d_1 = 10\%$ and $d_2 = 60\%$ of the current frame spray penetration as referenced in Figure 6.

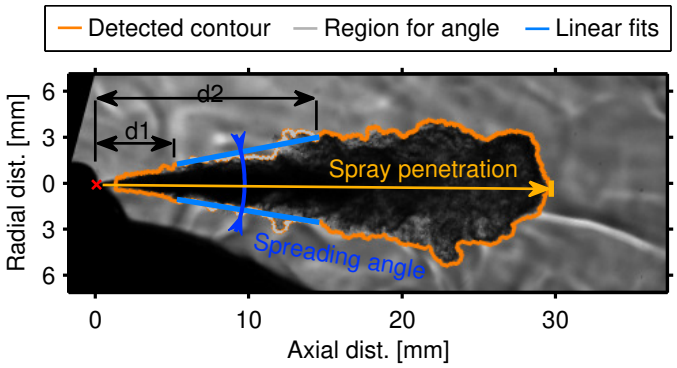

Figure 6: Macroscopic spray variables extracted from the contour analysis. The frame shown is at 560 µs after SOI, for a rail pressure of 100 MPa, a chamber density of 22.8 kg m^{-3} and temperature of 800 K.

3. Results and discussion

This section presents the results, first in terms of the image processing methodology for multiple injection strategies, and then the spray macroscopic variables.

3.1. Effect of the injected quantity on the spray segmentation

Increasing the injected quantity in pilot-main strategies might affect the contour detection algorithm. The first pulse could induce higher density gradients as more mass is being introduced into the test chamber, decreasing the density differences between injections that help to delimit their boundaries. Figure 7 presents a pilot-main strategy for a fixed dwell time and the two different pilot quantities studied. Each mass quantity is grouped and represented by four images that individually portray a separate time step. Overall, no apparent effect was observed between the injected mass of the first injection and the difficulty of spray segmentation of the second pulse, as shown in the figure. Increasing the pilot quantity introduced more disturbances in the test chamber, which implies a higher momentum flux that is translated into a higher injection velocity. Consequently, the first spray, penetrated a larger distance and was more diluted when met by the second pulse. Thus, the local density difference in the limiting border between injections was approximately the same.

3.2. Effect of the dwell time on the spray segmentation

A critical variable that affects spray segmentation in multiple injection strategies is the dwell time between pulses. As mentioned before, the closer the injections are, the higher the difficulty is for the image processing to properly decouple each event because the local density in the limits of the sprays is similar in schlieren imaging, as well as the light attenuation in DBI.

Figure 8 presents an example of the segmentation achieved for the four different dwell times studied, each grouped and represented by four images that individually portray a separate time step. It can be easily recognized that with decreasing dwell times, the density gradient between injections pulses, or in this

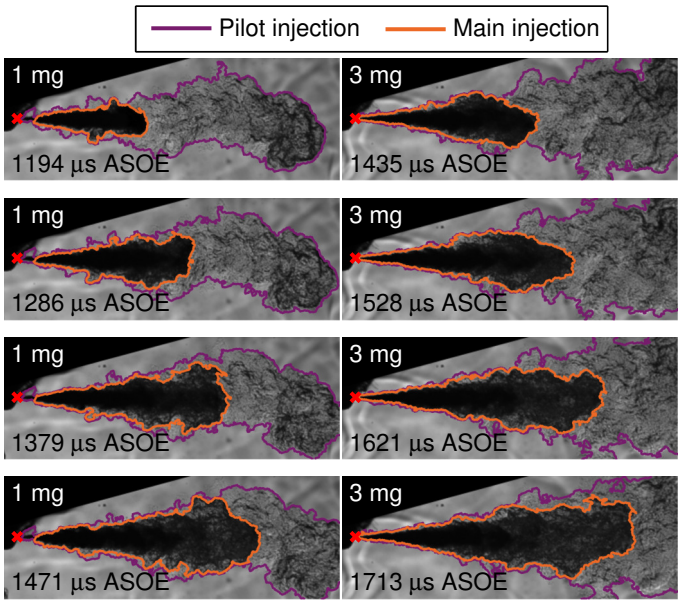

Figure 7: Example of the contour segmentation for different injected quantities. The frames shown are for a pilot-main event with a dwell time of 500 µs, a rail pressure of 100 MPa, a chamber density of 22.8 $\mathrm{kg\,m^{-3}}$ and temperature of 800 K.

case the difference in pixel intensity, becomes significantly lower. Consequently, for a dwell time of 200 µs, the contour obtained is not as smooth as the one depicted for 650 µs, and the segmentation of the second injection is more likely to sometimes over-predict spray penetration values. Therefore, precise tuning was needed for these cases to get acceptable results. Nevertheless, the contours depicted for the second injection pulse were, in general, remarkably well delimited.

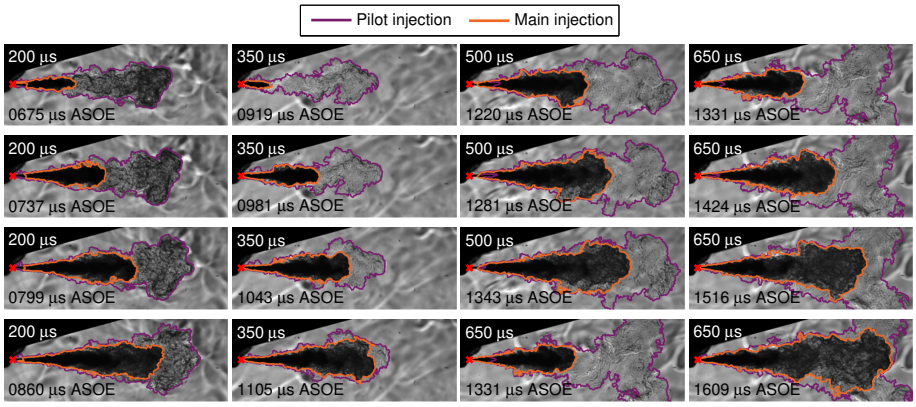

Figure 8: Example of the contour segmentation for different dwell times. The frames shown are for 1-29 mg pilot-main events, a rail pressure of 200 MPa, a chamber density of 22.8 kg m^{-3} and temperature of 800 K.

3.3. Liquid phase penetration for multiple injection strategies

The effects that traditional boundary conditions have on the spray evaporation of single injection pulses are well-known [19, 28, 30], and therefore are not presented in this article. Firstly, liquid length decreases with increasing chamber temperature, as the hotter gases provide more energy reducing the distance required for the fuel to fully vaporize. Secondly, liquid length decreases with increasing density, as more gas is entrained due to a wider spreading angle, and more energy for vaporization is available. Lastly, rail pressure has no apparent influence on the liquid length; as the jet velocity increases at higher injection pressures, the higher rate of air entrainment supplies enough energy to maintain

the evaporation distance constant.

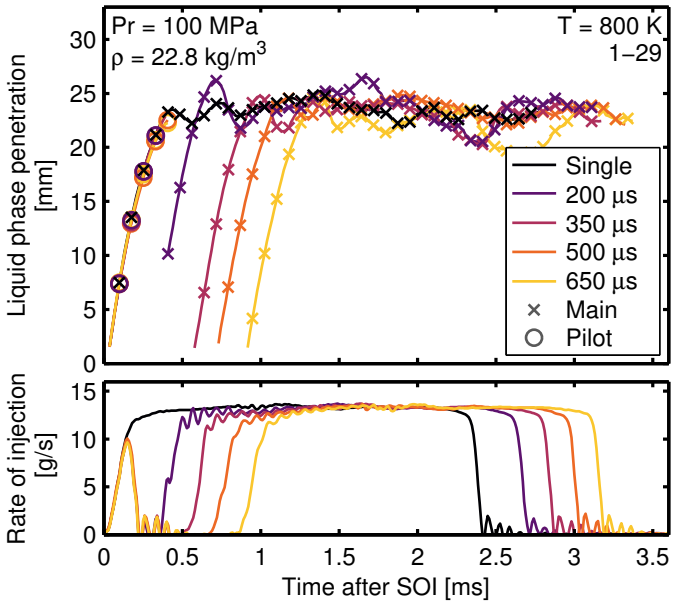

Figure 9: Liquid phase penetration for a pilot injected quantity of 1 mg. Symbols depict the spray segmentation of the pilot and main injections.

Examples of the liquid phase penetration results for different dwell times and both pilot quantities are presented in Figures 9 and 10. Symbols depict each of the injection pulses.

From the figures, neither the pilot quantity nor its hydraulic separation affected the liquid phase penetration of the main pulse, corresponding to results found in the literature [31]. This trend is somewhat expected in these types of experimental vessels, where the chamber volume is quite large. Therefore, air entrained by the spray provides more or less the same energy (temperature) to the fuel. In test cells with smaller volumes that resemble engine geometries, the liquid length of a second pulse might increase. This strongly depends on the re-entrainment of vapor structures at the edge of the jet [9], left over by the previous injection. The viscosity, which differs among different fuels, could also alter the jet's behavior during multiple injections, specifically in the case of a short dwell time. Yu et al. [32] discovered that a lower viscosity fuel,

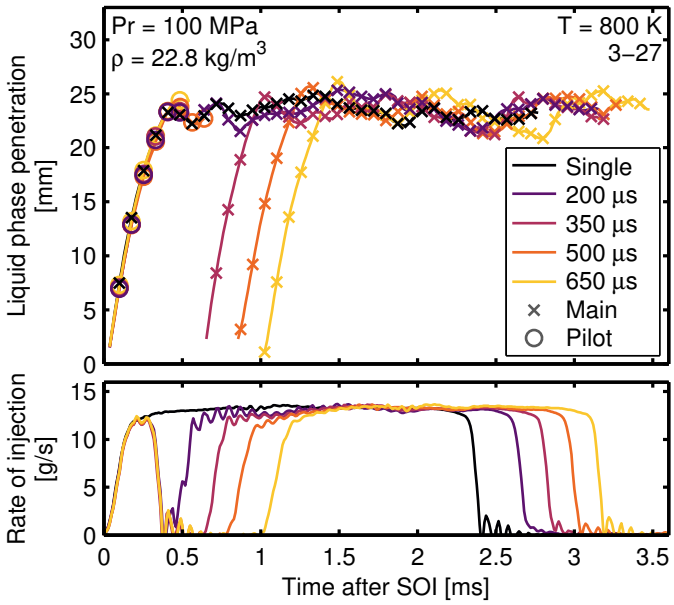

Figure 10: Liquid phase penetration for a pilot injected quantity of 3 mg. Symbols depict the spray segmentation of the pilot and main injections. The main event was manually decoupled for a dwell time of 200 µs for visualization purposes.

kerosene, compared to diesel, exhibited longer injection durations since a higher momentum signal was detected. Both pilot masses reach the same liquid phase penetration as the main injection, but only with 3 mg the penetration briefly achieved stabilized values. In general, the start of injection values extrapolated from the main injection were remarkably well correlated with those from the rate of injection measurements [7].

Results were summarized by calculating the average value in the stabilized region of the main injection, or liquid length, and presented in Figure 11. The x-axis displays the real chamber temperature, not the nominal value, calculated as the average value during the measurement of all the repetitions. No differentiation for rail pressure was done for the plot because it is known it does not affect liquid length. As stated before, both the quantity and dwell time of the pilot injection showed no impact on the stationary liquid length of the main pulse, at least considering the precision of this experimental diagnostics, as results are grouped mainly by chamber conditions.

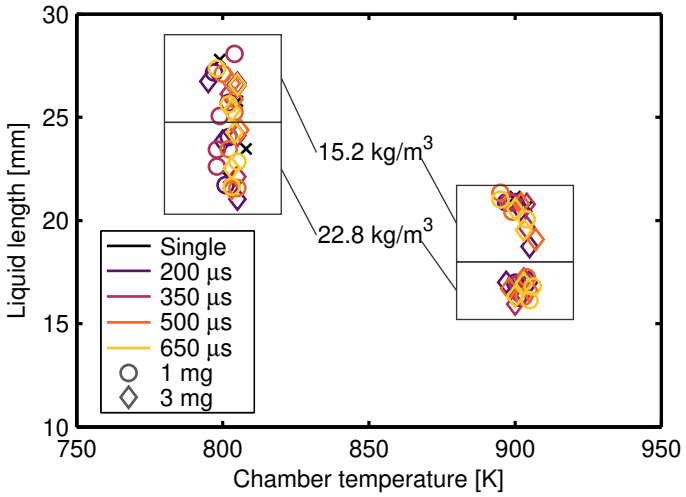

Figure 11: Time-averaged liquid length of the main injection for all conditions tested. Single injections are depicted with a cross symbol. Rectangles group conditions with the same chamber density.

An example of the liquid phase penetration results for different dwell times

and both post injected quantities are shown in Figure 12. Symbols depict the different injections pulses, and dashed lines represent post mass of 3 mg. Strategies with dwell times of 200 and 350 µs could not be decoupled, as only one more extended injection event was visible. In general, as before, no influence was observed from the main on the post injection liquid phase penetration.

Overall, it was observed that the secondary injection depicted a higher penetration rate than the prior pulse.

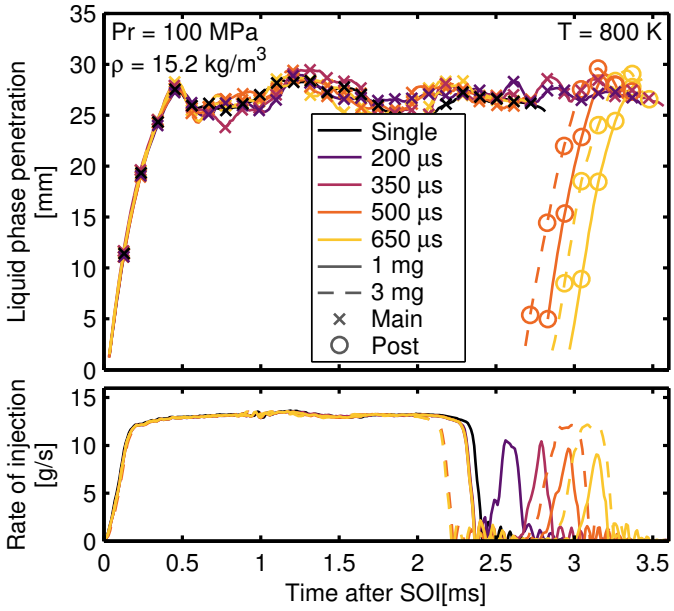

Figure 12: Liquid phase penetration for both post injected quantities. Symbols depict the spray segmentation of the main and post injections, and the dashed lines represent the post mass of 3 mg. Strategies with hydraulic dwell times of 200 and 350 µs could not be decoupled.

3.4. Vapor phase penetration for multiple injection strategies

As previously stated, the effects that traditional boundary conditions have on the spray development of single injection pulses are well-documented [25, 27, 28, 33], and are therefore not presented in this document. Firstly, vapor spray penetration increases with increasing injection pressure, as an initial higher kinetic energy is provided to the spray in terms of velocity, as observed from

momentum flux measurements. Secondly, vapor spray penetration decreases with increasing chamber density, as the aerodynamic interactions between liquid and gas widen the spray and causing it to lose momentum more rapidly. Lastly, chamber temperature has no apparent affect on spray penetration, as it is mainly dominated by momentum flux and aerodynamic phenomena.

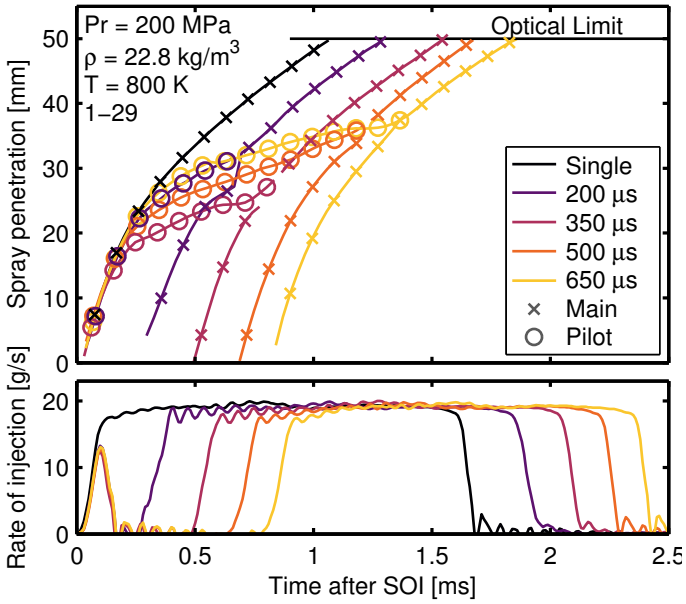

Figure 13: Spray penetration for a pilot injected quantity of 1 mg. Symbols depict the spray segmentation of the pilot and main injections.

Examples of the results for different dwell times and both pilots injected quantities are presented in Figures 13 and 14, and were optically limited by the field of view that was 50 mm. Symbols depict the different injection pulses. As in the previous sections, the SOI of the main injection correlated remarkably well with ROI measurements. Increasing the pilot quantity shifted the transition zone, where the main injection caught up to the pilot downstream of the spray development. The higher momentum flux of the 3 mg pilot enabled it to penetrate farther into the chamber, hence when the main injection started it was already beyond the optical limit. The spray penetration of the main pulse was somewhat affected by the dwell time. As the pilot injection initially ac-

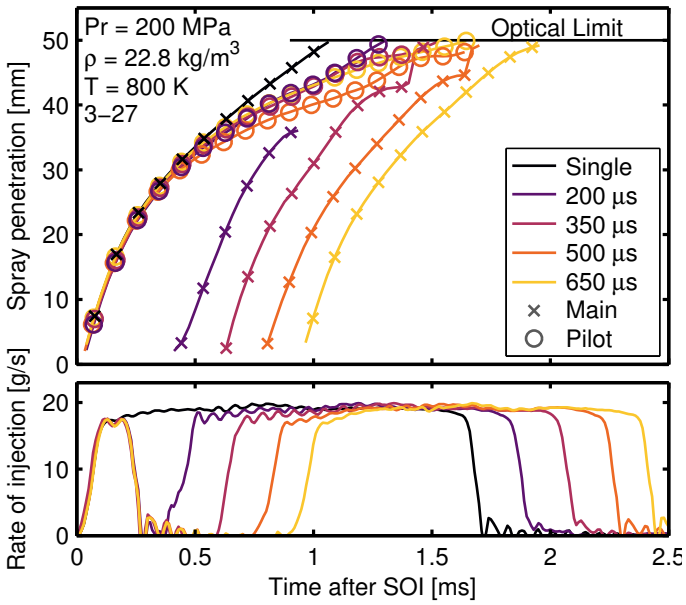

Figure 14: Spray penetration for a pilot injected quantity of 3 mg. Symbols depict the spray segmentation of the pilot and main injections.

celerates the stationary gas in the combustion chamber [31, 34, 35], the second pulse loses less momentum enabling it to penetrate faster than the reference case, increasing the mixing rate at the head of the spray [34]. Wang [35] called this phenomenon induced air driving force, concluding that a shorter dwell time contributes to a stronger induced driving force. Contrarily, an extended dwell leads to a weaker driving force, as more time is provided for the gas to decelerate. The main injection could also experience a higher spray penetration rate resulting from a higher momentum induced by the previous injection if the timing of the main injection was incident with a high point in the pressure wave signal that is traveling through the rail [36].

To isolate the effect of the dwell time on the acceleration of the spray development, Figure 15 presents the penetration of the main pulse shifted to the same origin as the reference single injection strategy, with the pilot pulses removed for visualization purposes. Only test points with 3 mg presented a somewhat more evident trend, probably due to the difficulty of quantifying such a sensitive

variable with the shot-to-shot dispersion of the 1 mg quantity. The figure depicts the trend mentioned previously; the rate of penetration of the main pulse increases with a pilot injection and a decreasing dwell time, due to the higher air driving force.

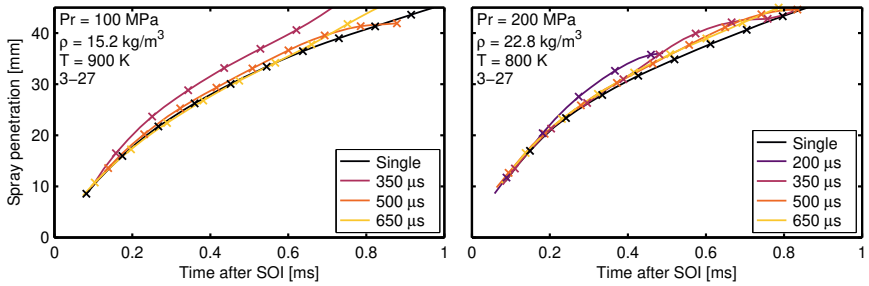

Figure 15: Differences of the rate of spray penetration of the main pulse compared to the single injection strategy for different dwell times. The curves were shifted to the same time origin for visualization purposes.

An example of the spray penetration results for different dwell times and both post injected quantities is condensed in Figure 16. Symbols depict the different injection pulses and dashed lines represent post mass of 3 mg. Test points with dwell times of 200 and 350 µs could not be decoupled, as only one more extended injection event was visible. In this strategy, the transition zone was out of the optical limit. As a result, no difference was observed regarding the injected masses. Nevertheless, for the two dwell times of the post injection properly decoupled, the same trend as with the pilot strategy can be depicted, that of an increasing spray penetration rate with decreasing dwell time.

3.5. Liquid phase spreading angle for pilot-main strategies

The transient liquid phase spreading angle of the main injection was averaged during the stationary stage of the injection, and each test point was compared to the reference point, to analyze the effect of a pilot pulse. Consequently, results depict the variation in degrees between the conditions with a pilot pulse compared to the single injection case. Values for a rail pressure of 100 MPa are presented in Figure 17.

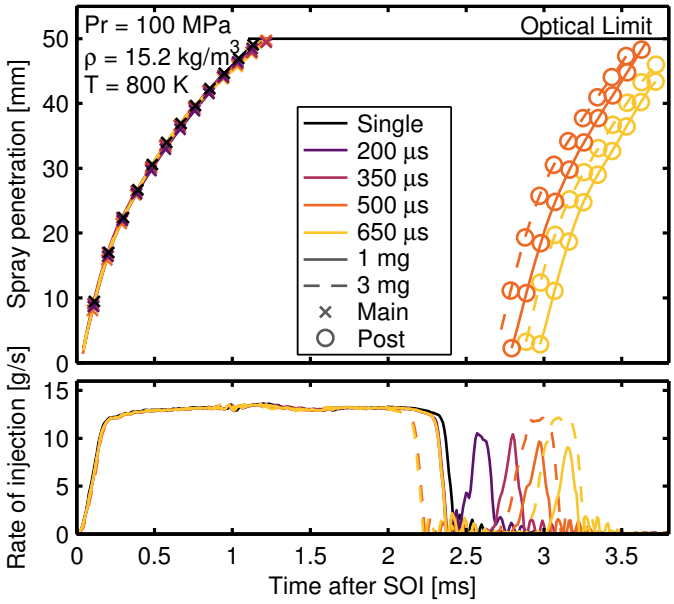

Figure 16: Spray penetration for both post injected quantities. Symbols depict the spray segmentation of the main and post injections, and the dashed lines represent the post mass of 3 mg. Strategies with hydraulic dwell times of 200 and 350 µs could not be decoupled.

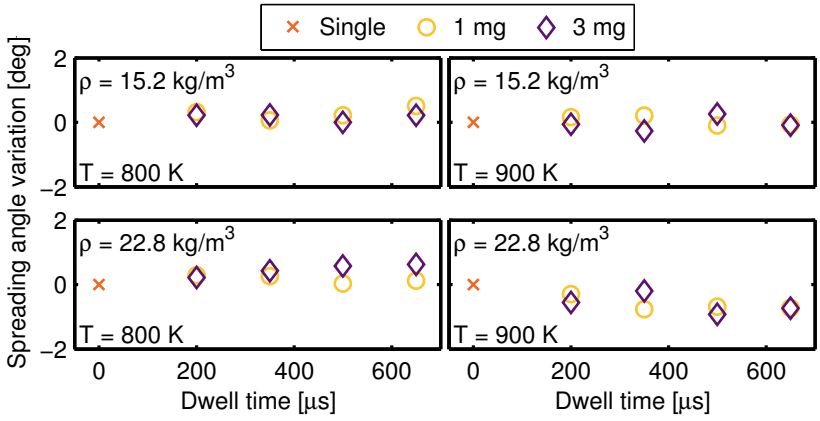

Figure 17: Effect of a pilot pulse on the liquid phase spreading angle of the main injection in terms of variation in degrees compared to the single injection case. Symbols depict different pilot quantities and the reference condition. All values depicted are for a rail pressure of 100 MPa.

From the figure, no trend was observed regarding the influence of the pilot injection on the spreading angle of the main pulse. Interestingly, even though the rate of penetration was higher with decreasing dwell time in the early spray development, liquid phase spreading angle remains more or less constant, as well as the liquid phase penetration. Therefore, this confirms that the rate of air entertainment is directly linked to the spray velocity and that the pilot pulse does not affect the liquid distribution of the main injection within the conditions tested.

3.6. Vapor phase spreading angle for pilot-main strategies

The same procedure as in the previous section was carried out to analyze the effect of a pilot pulse on the vapor spray spreading angle of the main injection. Values for a rail pressure of 100 MPa are presented in Figure 18.

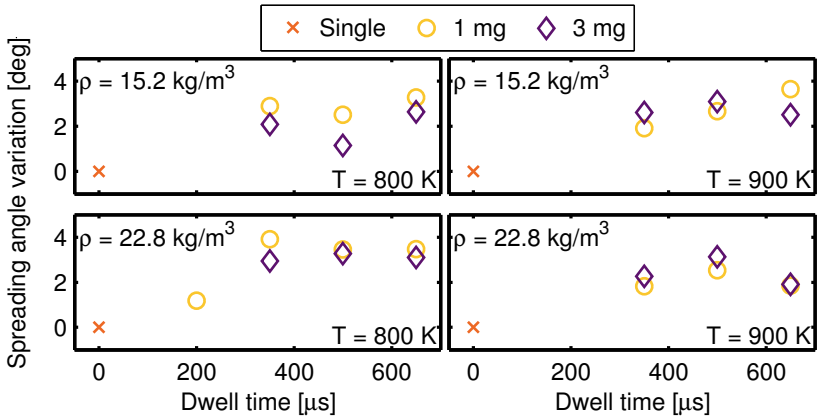

Figure 18: Effect of a pilot pulse on the spray spreading angle of the main injection in terms of variation in degrees compared to the single injection case. Symbols depict different pilot quantities and the reference condition. All conditions depicted are for a rail pressure of 100 MPa.

Calculations of the overall spray spreading angle measured through the vapor phase visualization can be significantly affected by the optical sensitivity and the image processing routines [27, 33]. Moreover, even though the spray tip was adequately segmented for the second pulse in the multiple injection cases,

the sides of the sprays were difficult to differentiate and properly decouple. Nevertheless, a general trend is observed as the spray spreading angle increases with a pilot pulse before the main. The second injection event is introduced into a somewhat stationary medium with a higher density and turbulence, induced by fuel of the first injection, and a higher angle is somewhat expected [10]. However, it is interesting to qualitatively observe that the main injection presents a higher rate of penetration even with a higher spreading angle. Nonetheless, the dependency on either the pilot quantity or dwell time is unclear and might be due to the uncertainties of the angle calculation in vapor contours.

4. 1-D Modeling and simulation of the thermal exchange in pilot-main strategy

One dimensional CFD tools have been extensively used in the prediction of spray behavior under engine-like conditions and could be extended to evaluate variables that are quite difficult to attain experimentally. They offer the advantage of a low computational cost due to the assumptions and simplifications adopted. A detailed description and analysis of the model could be found in [37]. The tool was used to predict the thermal interaction between two pulses. Two cases of different rail pressures were investigated, 100 MPa and 200 MPa, for the pilot-main strategy of 3-27. A similar calibration procedure to that in [37] was performed on the spray cone angles in order to fit the experimental data, in terms of vapor phase penetration and liquid length. Generally, a narrower spray cone angle is given in the near nozzle region and a wider one further downstream. Figure 19 shows the vapor spray penetration results for dwell times of 650 μs and 350 μs. It can be seen that the evolution of the vapor phase penetration remains within a close proximity of the experimental data for the pilot, changes slope after the EOI pilot, and finally catches up to the main injection penetration. The 200 MPa case also effectively captures the spray penetration evolution that could be seen to develop with a higher rate (steeper slope) compared to that of 100 MPa rail pressure.

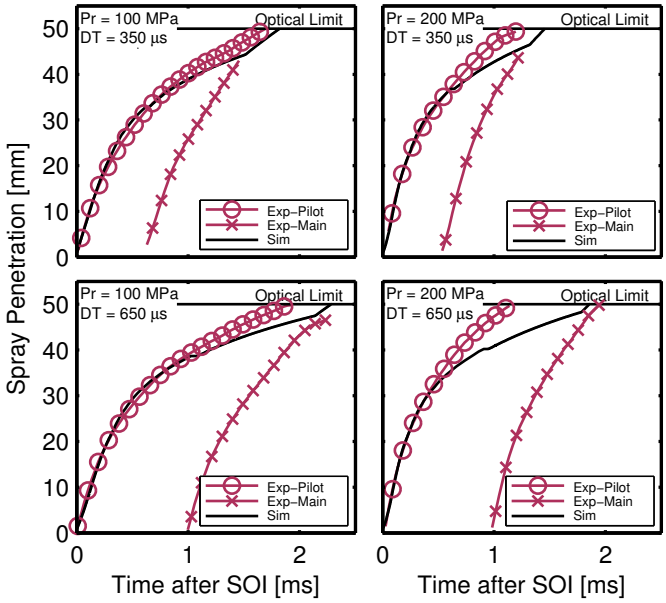

Figure 19: Vapor spray penetration results of 1D spray model and experimental measurements. Two different cases of rail pressures are depcited for two dwell times.

The verification of the 1D model for the multiple injection cases so far is ought to be done considering the liquid penetration length as well. The liquid length plays a significant role in thermal exchange analysis that will follow, since the main difference between the multiple injection and the single injection cases will be after the realization of the maximum liquid length of the spray. Liquid phase penetration results are displayed in Figure 20 along with the experimental data for the corresponding cases. The average liquid length in the stabilized region of the spray agrees with the experimental data.

The capability of the model to predict the liquid and vapor phase penetration permits the analysis of other computed parameters with confidence. The evolution of the temperature along the spray axis is shown in Figure 21. Three regions are depicted. Initially, the spray evolves from the injector at the injection temperature of 363 K and remains constant for the duration of the spray intact length. The second region exhibits an increase in the spray temperature due to entrainment of hot air in the chamber that is around 900 K and the

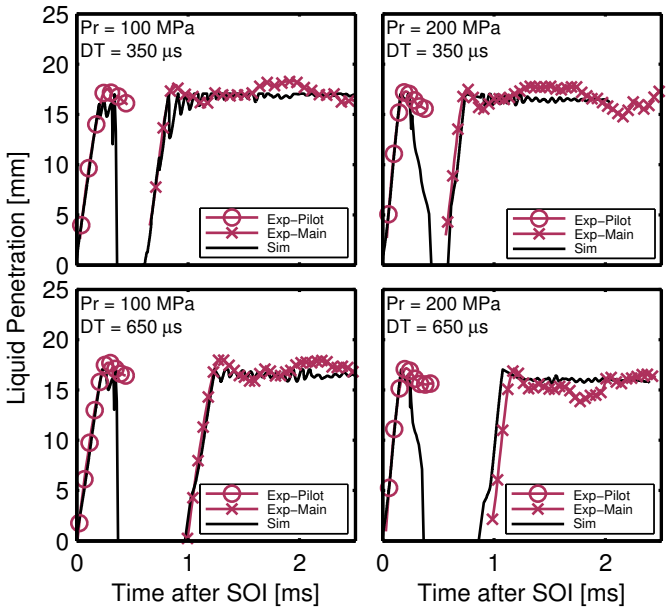

Figure 20: Liquid penetration results of 1D spray model and experimental measurements. Two different cases of rail pressures are depcited for two dwell times.

air enthalpy is used to vaporize the liquid fuel. A change in slope defines the third region where all the liquid has been vaporized and the enthalpy of the surrounding air is used mainly to increase the mixture temperature.

Both cases of injection pressure demonstrate the same trend, in which the single and both multiple injections increase with a similar temperature profile followed by a divergence of the 350 μs case. The first phase of the temperature profile could be associated with the rate at which air is entrained into the spray which is not directly linked with the occurrence of a pilot injection. This also agrees with what was explained in subsection 3.6 in which the spreading angle of the liquid phase remained constant, to some extent, not being influenced by the occurrence of a pilot injection. Hence, the heat transfer rate from the hot air to the liquid fuel in this phase is quite the same and not effected by the pilot, as evidenced by the overlapped curves. Further downstream the spray axis, a clear difference in temperature magnitude for the shorter dwell time is noticed compared to other two. Since the main injection is injected 350 μs after the

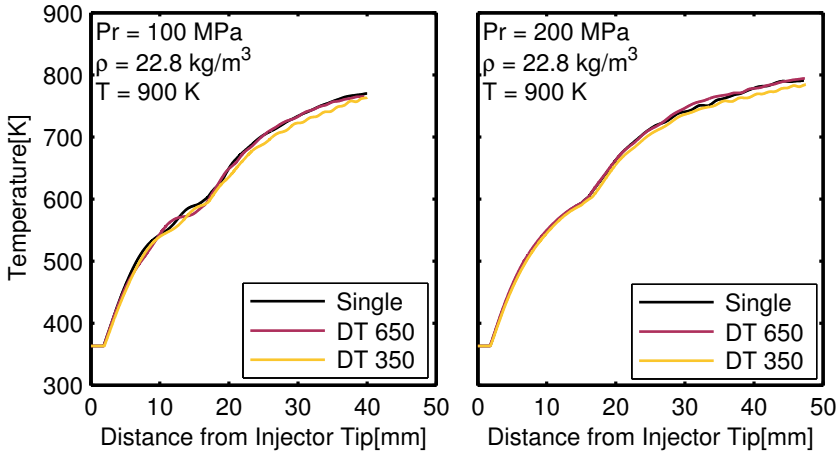

Figure 21: Axial spray temperature as a fucntion of axial distance from injector tip taken at 1 ms after the start of the main injection. Two different cases of rail pressures are depcited for two dwell times and the single injection case.

pilot, it is injected into a slightly colder environment induced by the evaporation of previous pulse. It is also interesting to note that for a longer dwell time, the effect of the pilot is not present on the main injection's temperature and the chamber conditions are somewhat restored to the initial conditions. However, it must be clearly noted that this could only be said for the assumption of a large chamber volume where the air far away from the nozzle is not effected by the spray development.

5. Summary and conclusions

In this paper, a novel image processing approach was proposed to depict two sprays that coexist in a single frame. This allowed to study the diesel spray macroscopic variables for multiple injection strategies in close coupled conditions in a non-reactive atmosphere. Measurements were carried out in an optically-accessible constant pressure and flow vessel, with a diffused back-illumination and a single-pass schlieren to visualize the liquid and vapor phase of the spray, respectively. The field of view allowed for an optical limit of 50 mm.

- Increasing the pilot quantity introduced more disturbances in the vapor. Nevertheless, it did not affect the spray segmentation of the second pulse, because the transition zone, where pulses overlapped, was pushed downstream from the nozzle. Consequently, the first pulse was already more diluted, which provided enough contrast in the frames to decouple both contours.
- Dwell time is a critical variable that affects spray segmentation in the optical diagnostics of multiple injection strategies. The closer the injections are, the higher the difficulty is to decouple each event, as the density gradient between pulses is much lower. As a consequence, finer tuning was needed to get acceptable results, but boundaries were remarkably well delimited.
- Neither the pilot mass quantity nor its hydraulic separation affected the stabilized liquid phase penetration of the main pulse, which was still mostly governed by chamber density and temperature.
- All pilot/post injections reached the same vaporization length as the main pulse.
- The first pulse accelerated the stationary gas in the combustion chamber, and as a consequence, the second event lost less momentum and penetrated faster than the reference single injection case. Pilot/post injections with higher mass depicted more evident trends, as they present less shot-to-shot variability.
- Pilot injections did not affect liquid phase spreading angle. Contrarily, vapor phase measurements with a pilot pulse showed an increase in the spreading angle compared to the reference case, probably caused by a higher localized density or turbulence from the previous injection. The effect of either the pilot quantity or dwell time was unclear, presumably due to the uncertainties of the angle calculation in vapor contours.

Acknowledgments

This research has been partially funded by Spanish Ministerio de Ciencia, Innovación y Universidades through project RTI2018-099706-B-100. Addition-

ally, the experimental hardware was purchased through FEDER and Generalitat Valenciana under project IDIFEDER/2018/037.

References

[1] J. Benajes, J. Martín, A. García, D. Villalta, A. Warey, Swirl ratio and post injection strategies to improve late cycle diffusion combustion in a light-duty diesel engine, Applied Thermal Engineering 123 (2017) 365–376. doi:10.1016/j.applthermaleng.2017.05.101.

[2] J. O'Connor, M. P. B. Musculus, L. M. Pickett, Effect of post injections on mixture preparation and unburned hydrocarbon emissions in a heavy-duty diesel engine, Combustion and Flame 170 (2016) 111–123. doi:10.1016/j.combustflame.2016.03.031.

[3] D. Schöppe, C. Stahl, G. Krüger, V. Dian, Servo-Driven Piezo Common Rail Diesel Injection System, ATZ Autotechnology 12 (2012) 42–47. doi:10.1365/s35595-012-0107-y.

[4] Y. Liu, R. D. Reitz, Optimizing HSDI Diesel Combustion and Emissions Using Multiple Injection Strategies, SAE Technical Paper 2005-01-0212 (2010). doi:10.4271/2005-01-0212.

[5] B. Chen, L. Feng, Y. Wang, T. Ma, H. Liu, C. Geng, M. Yao, Spray and flame characteristics of wall-impinging diesel fuel spray at different wall temperatures and ambient pressures in a constant volume combustion vessel, Fuel 235 (2019) 416–425. URL: https://doi.org/10.1016/j.fuel.2018.07.154. doi:10.1016/j.fuel.2018.07.154.

[6] H. Liu, B. Chen, L. Feng, Y. Wang, W. Yi, M. Yao, Study on fuel distribution of wall-impinging diesel spray under different wall temperatures by laser-induced exciplex fluorescence (LIEF), Energies 11 (2018) 1–14. doi:10.3390/en11051249.

[7] R. Payri, J. Gimeno, P. Marti-Aldaravi, A. Viera, Measurements of the mass allocation for multiple injection strategies using the rate of injection and momentum flux signals, International Journal of Engine Research (2019). doi:10.1177/1468087419894854.

[8] J. V. Pastor, J. J. López, J. M. García-Oliver, J. M. Pastor, A 1D model for the description of mixing-controlled inert diesel sprays, Fuel 87 (2008) 2871–2885. doi:10.1016/j.fuel.2008.04.017.

[9] L. M. Pickett, S. Kook, T. C. Williams, Transient Liquid Penetration of Early-Injection Diesel Sprays, SAE International Journal of Engines 2 (2009) 2009–01–0839. doi:10.4271/2009-01-0839.

[10] M. J. Borz, Y. Kim, J. O'Connor, The Effects of Injection Timing and Duration on Jet Penetration and Mixing in Multiple-Injection Schedules, SAE Technical Paper 2016-01-0856 (2016). doi:10.4271/2016-01-0856.

[11] R. Payri, J. Gimeno, S. Cardona, S. Ayyapureddi, Experimental study of the influence of the fuel and boundary conditions over the soot formation in multi-hole diesel injectors using high-speed color diffused back-illumination technique, Applied Thermal Engineering 158 (2019) 113746. doi:10.1016/j.applthermaleng.2019.113746.

[12] R. Payri, J. Gimeno, S. Cardona, S. Ayyapureddi, Measurement of Soot Concentration in a Prototype Multi-Hole Diesel Injector by High-Speed Color Diffused Back Illumination Technique, SAE Technical Paper 2017-01-2255 (2017). doi:10.4271/2017-01-2255.

[13] R. S. G. Baert, P. J. M. Frijters, B. Somers, C. C. M. Luijten, W. D. Boer, W. De Boer, Design and operation of a high pressure, high temperature cell for HD diesel spray diagnostics: guidelines and results, SAE Technical Paper 2009-01-0649 (2009). doi:10.4271/2009-01-0649.

[14] M. Meijer, B. Somers, J. E. Johnson, J. D. Naber, S.-Y. Lee, L. M. Malbec, G. Bruneaux, L. M. Pickett, M. Bardi, R. Payri, T. Bazyn, Engine Com-

bustion Network (ECN): Characterization and Comparison of Boundary Conditions for Different Combustion Vessels, Atomization and Sprays 22 (2012) 777–806. doi:10.1615/AtomizSpr.2012006083.

[15] A. Viera, Effect of multiple injection strategies on the diesel spray formation and combustion using optical diagnostics, Ph.D. thesis, Universitat Politècnica de València, 2019.

[16] R. Payri, J. M. García-Oliver, M. Bardi, J. Manin, Fuel temperature influence on diesel sprays in inert and reacting conditions, Applied Thermal Engineering 35 (2012) 185–195. doi:10.1016/j.applthermaleng.2011.10.027.

[17] Engine Combustion Network, https://ecn.sandia.gov/diesel-spray-combustion/, Online, 2010.

[18] R. Payri, J. Gimeno, C. Mata, A. Viera, Rate of injection measurements of a direct-acting piezoelectric injector for different operating temperatures, Energy Conversion and Management 154 (2017) 387–393. doi:10.1016/j.enconman.2017.11.029.

[19] D. L. Siebers, Liquid-Phase Fuel Penetration in Diesel Sprays, SAE Technical Paper 980809 (1998). doi:10.4271/980809.

[20] R. Payri, G. Bracho, P. Martí-Aldaraví, A. Viera, Near field visualization of diesel spray for different nozzle inclination angles in non-vaporizing conditions, Atomization and Sprays 27 (2017) 251–267. doi:10.1615/AtomizSpr.2017017949.

[21] L. M. Pickett, C. L. Genzale, J. Manin, L.-M. Malbec, L. Hermant, Measurement Uncertainty of Liquid Penetration in Evaporating Diesel Sprays, in: ILASS Americas, 23rd Annual Conference on Liquid Atomization and Spray Systems, May, ILASS-Americas, Ventura, CA (USA), 2011.

[22] J. Benajes, R. Payri, M. Bardi, P. Martí-Aldaraví, Experimental characterization of diesel ignition and lift-off length using a single-hole ECN

injector, Applied Thermal Engineering 58 (2013) 554–563. doi:10.1016/j.applthermaleng.2013.04.044.

[23] R. Payri, F. J. Salvador, J. Manin, A. Viera, Diesel ignition delay and lift-off length through different methodologies using a multi-hole injector, Applied Energy 162 (2016) 541–550. doi:10.1016/j.apenergy.2015.10.118.

[24] J. V. Pastor, R. Payri, J. M. García-Oliver, F. J. Briceño, Schlieren Methodology for the Analysis of Transient Diesel Flame Evolution, SAE International Journal of Engines 6 (2013) 2013–24–0041. doi:10.4271/2013-24-0041.

[25] R. Payri, J. Gimeno, G. Bracho, D. Vaquerizo, Study of liquid and vapor phase behavior on Diesel sprays for heavy duty engine nozzles, Applied Thermal Engineering 107 (2016) 365–378. doi:10.1016/j.applthermaleng.2016.06.159.

[26] J. V. Pastor, R. Payri, J. M. García-Oliver, J.-G. Nerva, Schlieren Measurements of the ECN-Spray A Penetration under Inert and Reacting Conditions, SAE Technical Paper 2012-01-0456 (2012). doi:10.4271/2012-01-0456.

[27] R. Payri, F. J. Salvador, G. Bracho, A. Viera, Differences between single and double-pass schlieren imaging on diesel vapor spray characteristics, Applied Thermal Engineering 125 (2017) 220–231. doi:10.1016/j.applthermaleng.2017.06.140.

[28] R. Payri, J. P. Viera, V. Gopalakrishnan, P. G. Szymkowicz, The effect of nozzle geometry over the evaporative spray formation for three different fuels, Fuel 188 (2017) 645–660. doi:10.1016/j.fuel.2016.06.041.

[29] F. R. Westlye, K. Penney, A. Ivarsson, L. M. Pickett, J. Manin, S. A. Skeen, Diffuse back-illumination setup for high temporally resolved extinction imaging, Applied Optics 56 (2017) 5028. doi:10.1364/AO.56.005028.

[30] D. L. Siebers, Scaling liquid-phase fuel penetration in diesel sprays based on mixing-limited vaporization, SAE Technical Paper 1999-01-0528 (1999). doi:10.4271/1999-01-0528.

[31] K. Karimi, Characterisation of Multiple-Injection Diesel Sprays at Elevated Pressures and Temperatures, Ph.D. thesis, University of Brighton, 2007.

[32] W. Yu, W. Yang, K. Tay, B. Mohan, F. Zhao, Y. Zhang, Macroscopic spray characteristics of kerosene and diesel based on two different piezoelectric and solenoid injectors, Experimental Thermal and Fluid Science 76 (2016) 12–23. URL: http://dx.doi.org/10.1016/j.expthermflusci.2016.03.008. doi:10.1016/j.expthermflusci.2016.03.008.

[33] L. M. Pickett, J. Manin, C. L. Genzale, D. L. Siebers, M. P. B. Musculus, C. A. Idicheria, Relationship Between Diesel Fuel Spray Vapor Penetration/Dispersion and Local Fuel Mixture Fraction, SAE International Journal of Engines 4 (2011) 2011–01–0686. doi:10.4271/2011-01-0686.

[34] G. Bruneaux, D. Maligne, Study of the Mixing and Combustion Processes of Consecutive Short Double Diesel Injections, SAE International Journal of Engines 2 (2009) 2009–01–1352. doi:10.4271/2009-01-1352.

[35] Z. Wang, Experimental study on diesel spray with single and multiple injection under room temperature and low temperature, Ph.D. thesis, University of Birmingham, 2015.

[36] W. Yu, W. Yang, B. Mohan, K. L. Tay, F. Zhao, Macroscopic spray characteristics of wide distillation fuel (WDF), Applied Energy 185 (2017) 1372–1382. URL: http://dx.doi.org/10.1016/j.apenergy.2015.12.051. doi:10.1016/j.apenergy.2015.12.051.

[37] J. V. Pastor, J. M. García-Oliver, J. M. Pastor, W. Vera-Tudela, One-dimensional diesel spray modeling of multicomponent fuels, Atomization and Sprays 25 (2015) 485–517. doi:10.1615/AtomizSpr.2014010370.